Improved Light Uniformity From Light-Emitting Diodes by Heterogeneous Microlenses and 3-D Printed Mold

Cheng-Han Chiang and Guo-Dung John Su

***Abstract*—We present a novel design and fabrication process using the hydrophilic confinement effect and a 3-D printer for producing convex and concave microlenses on top of light-emitting diodes. We use energy conservation and a lawnmower algorithm to design a freeform lens, and transform it into heterogeneous microlenses. The diameters of the microlenses on top of the light-emitting diode are 500 and 200 μm for the concave and convex shapes, respectively. Heterogeneous microlenses are printed on a glass substrate using the hydrophilic confinement effect of SU-8 photoresist and an inkjet printer. Then, the array is copied with a mold made by a 3-D printer for the replication process. In the replication process, the mold is filled with polydimethylsiloxane to reproduce heterogeneous microlenses. Experimental results show that this heterogeneous microlens array improves the light distribution uniformity of a light-emitting diode from 17% to 63%.**

***Index Terms*—Freeform lens, light-emitting diode (LED), microlenses, micro-structure on LED.**

I. Introduction

LIGHT emitting diodes (LEDs) can be found in applications ranging from traffic lights and street lighting to indoor lighting and appliances. [1]. The strength of the LED lies in its small volume, long application life, energy efficiency, and durability [2]. One high-volume application of LEDs is in the backlighting unit (BLU) of a liquid crystal display (LCD). The backlight structures of LCDs are categorized according to two frameworks based on their illuminance distribution positions: the edge-lit form and the direct-lit form. Both forms are used to achieve uniform light distribution [3], [4]. Most of the micro/nano structures on LEDs in previous works [5]–[7], however, are designed to enhance the light extraction efficiency. Unlike other lighting technologies, LED emissions tend to be directional, which can be either advantageous or disadvantageous, depending on the application. In a BLU, the light distribution of the LEDs is important. Previous efforts to improve lighting uniformity have depended on either bulky optical components [8] or expensive patterning processes [9], [10]. As a result, the backlight units for LCDs need either light guide plates or diffusers to achieve high uniformity. These two components are used to re-distribute the light intensity, which causes additional light loss. To compensate for the loss, more LED chips are used, which results in higher power consumption.

In order to optimize the light distribution uniformity of LEDs, we have designed a non-imaging system [11] based on a freeform surface. It has micro structures on top of a single LED chip, which are compatible with existing LEDs. We use micro structures to replace the guide plates and diffusers. This design also reduces the required number of LEDs and the dimensions of the backlight unit.

A freeform surface differs from the traditional imaging optics surface in that it does not have a single analytic expression, and the curved surface is constructed of discrete points. Compared to the traditional optics surface, a freeform surface can reduce the volume of the whole optical system and achieve better effects with fewer optical components.

Freeform surfaces have countless advantages. However, their fabrication requires ultra-high precise manufacturing techniques; otherwise, their performance will be significantly affected. The footprint of an LED chip, usually less than 1 mm^2, makes it challenging to produce a freeform surface on an LED chip with traditional machining tools. In order to prevent difficulties in the manufacturing process and to reduce the volume of the entire illumination system, heterogeneous microlenses made by micromachining have been considered. A freeform surface can re-distribute light rays to corresponding positions because the curvature can be optimized in different places. Another option is to use heterogeneous microlenses, which can be fabricated with various focal lengths to simulate the effect of varying optical power in a freeform lens and to make the illumination uniform. In fact, a heterogeneous microlens can be viewed as a discrete freeform surface lens.

In this paper, we describe the design of heterogeneous microlenses based on a freeform surface. We started by constructing a freeform lens. Then we made heterogeneous microlenses based on the curvature of the freeform lens at different locations. The hydrophilic confinement effect of SU-8 photoresist and a 3-D printer were used to fabricate the microlenses. Fig. 1 illustrates the working principle of the microlens array. Finally, we experimentally demonstrated the high uniformity of the LED output with heterogeneous microlenses. To the best of our knowledge, this is the first time that 3-D micro structures on top of LEDs have been fabricated by printing technologies to improve light uniformity.

Manuscript received October 1, 2014; revised November 24, 2014; accepted December 14, 2014. Date of publication December 22, 2014; date of current version January 26, 2015.

The authors are with the Graduate Institute of Photonics and Optoelectronics, National Taiwan University, Taipei 10617, Taiwan (e-mail: r01941107@ntu.edu.tw; gdjsu@cc.ee.ntu.edu.tw).

Color versions of one or more of the figures in this paper are available online at http://ieeexplore.ieee.org.

Digital Object Identifier 10.1109/JSTQE.2014.2382972

1077-260X © 2014 IEEE. Translations and content mining are permitted for academic research only. Personal use is also permitted, but republication/redistribution requires IEEE permission. See http://www.ieee.org/publications_standards/publications/rights/index.html for more information.

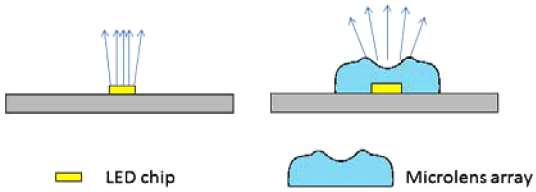

Fig. 1. Using the microlens array to improve the light distribution uniformity.

II. Design and Simulation

Before fabricating the microlens array, we started by designing a freeform surface and transferring it into the microlens array. The variable separation mapping design method [11] was applied to construct a freeform surface. Using the lawnmower algorithm, we obtained the distances from the LED to all points on all latitudes. We calculated all points on the freeform surface, which allowed us to redistribute the light intensity from an LED uniformly onto a square surface. Afterward, we adjusted the sizes and curvature radii of the microlenses according to the simulation results. By repeating an optimization process, a similar effect was obtained. All design steps are explained below in detail.

A. Design of a Freeform Surface

We utilized the energy conservation equation to obtain the corresponding relationship of the coordinates on the target plane. In order to get the relationship of the average energy *E* on the target plane and the normal direction of intensity I_o of the LED light source, we adopted the relationship that the total flux of the light source equaled the total energy on the target plane. In terms of mathematics, the coordinates of the freeform surface and target plane were spherical coordinates (θ, φ) and rectangular coordinates (*x*, *y*), respectively. The following formula can be used to express such a physical relationship:

$$\int_0^{\theta}\int_0^{\phi} I(\theta,\phi)\sin\varphi d\varphi d\theta = \int EdA. \tag{1}$$

In formula (1), the right side is the expression of energy in a unit cell, and *E* is the required average energy of the target plane. On the left side, θ is the angle between the vector projection on the *xy* plane and the positive *x*-axis, and φ is the angle between the vector and the positive *z*-axis. *dA* is the tiny area on the target plane. With formula (1), the relation of luminous intensity I_o and average energy *E* in the target plane were obtained:

$$E = \frac{I_0 \times \pi}{4 \times L_x \times L_y}. \tag{2}$$

We divided the angle into $\mathrm{m} \times \mathrm{n}$ cells. On the corresponding target plane, the distances at the direction positive *x*-axis vector and direction positive-*y*-vector were also divided into $\mathrm{m} \times \mathrm{n}$ cells such that there were $\mathrm{m} \times \mathrm{n}$ cells on the whole target plane. Subject to the corresponding relationship in Fig. 2 and formulas (1) and (2), the variables in the corresponding relationship between freeform surface and target plane can be shown as the following formulae [12]:

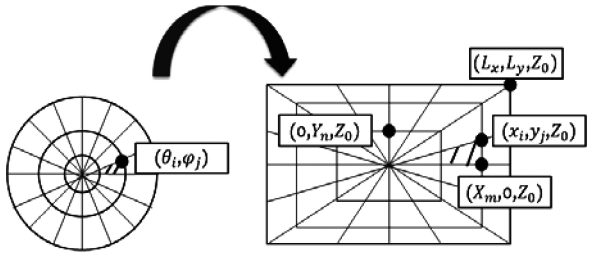

Fig. 2. Corresponding relationships between the coordinates on the target plane and the coordinates on the freeform surface.

$$y = 4 \times \frac{\theta_i}{\pi} \times Y, \quad 0 \le \theta_i \le \frac{\pi}{4} \tag{3}$$

$$x = \left(4 - 4 \times \frac{\theta_i}{\pi}\right) \times X, \quad \frac{\pi}{4} \le \theta_i \le \frac{\pi}{2}. \tag{4}$$

In the formula, *X* and *Y* are the values of the positive-*x*-axis and the positive-*y*-axis of the target plane, respectively, and θ_i is the angle θ of the number *i*. L_x and L_y are the values of the end of the boundary positive-*x*-axis and the end of the boundary positive-*y*-axis of the target plane, respectively. Accordingly, φ_j is the angle φ of the number *j*. In the following figure, X_m and Y_n are the values of the boundary positive-*x*-axis for the number *m* and the boundary positive-*y*-axis for the number *n*, respectively; x_i and y_j are the value of the *x* coordinate with corresponding θ_{i} and the value of the *y* coordinate with corresponding φ_j, respectively

$$X \times Y = L_x \times L_x \times (\sin\varphi_i)^2 \tag{5}$$

$$\frac{X}{Y} = \frac{L_x}{L_y}. \tag{6}$$

Then we used a lawnmower algorithm [13], an iteration process, to derive other points on the surface under the premise that the original condition surface point is known. The derivation is based on the fact that a small plane for the initial points intersects its adjacent small plane along a line defined by the bisector of the other two vectors as the bisectors hitting the first elemental plane at a distance. Therefore, the distance to the next point on the surface can be obtained in a similar way. In the end, the lawnmower algorithm yielded the distances from all points to the origin on the 1st longitude. Then, all points on this longitude were taken as the initial points on every latitude, as shown in Fig. 3. Thus, from all the points on the freeform surface, we could construct the desired freeform surface [13], [14].

B. Transformation of a Freeform Lens Into a Microlens Array

In the freeform surface design, we assumed the height from the target plane to the origin was 2 mm; the rectangular target plane (RTP) was $3\,\mathrm{mm} \times 3\,\mathrm{mm}$. The dimensions of the LED source were $200\,\mu\mathrm{m} \times 200\,\mu\mathrm{m}$. The square freeform surface was $1.73\,\mathrm{mm} \times 1.73\,\mathrm{mm}$ and 1 mm away from the origin. Since manufacturing such a small freeform surface is extremely difficult, microlens arrays were considered for use as the freeform

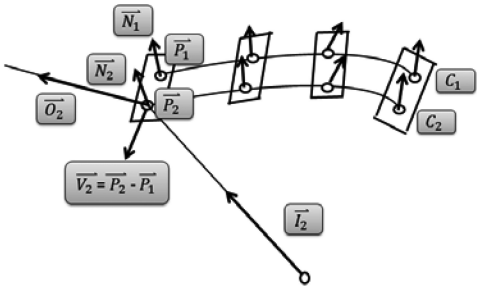

Fig. 3. Calculation of points on C_2 at the tangent plane of points on C_1.

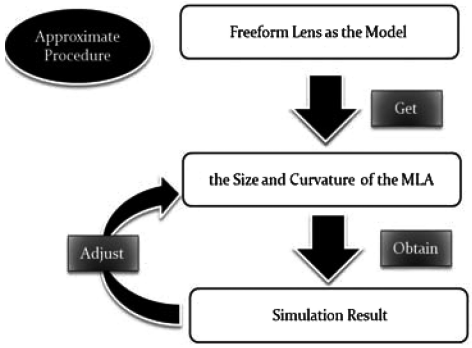

Fig. 4. Approximate process of transferring freeform lens to micro lens arrays.

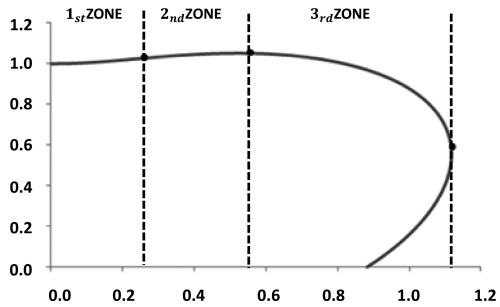

Fig. 5. Cross-sectional view of a freeform surface from center to edge; Z coordinate versus X coordinate.

surface. In other words, a microlens array can be viewed as a discrete freeform surface lens. We adjusted the size and curvature radius of the microlenses according to the simulated results. Then, by repeating an optimization process, a similar effect was obtained, as shown in Fig. 4

To explain how this approximation process works, the freeform surface in the previous section is used as an example. The simulated result of the freeform lens was as follows: length and width = 1.73 mm, and height = 1 mm. Fig. 5 represents the relationship of a z coordinate corresponding to an x coordinate. At first, we classified the curvature radius from negative to zero, as we had done in the first zone. We continued by classifying the radius of curvature values from 0 to the maximum z coordinate, as we had done in the second zone. In the last step, the point of the maximum value of the z coordinate

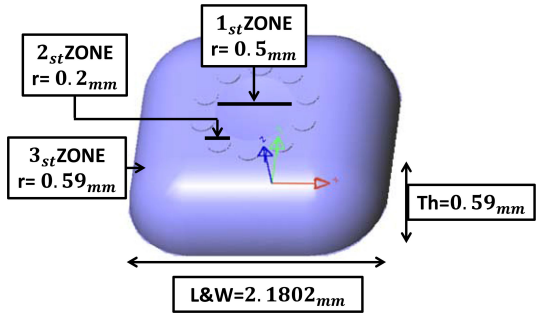

Fig. 6. The dimensions of heterogeneous microlenses after optimization from a freeform surface.

to the maximum value of the x coordinate was classified, as we had done in the third zone.

With respect to optimization, LightTools software and damped least squares algorithms were used. The original microlens array was imported for a simulation. Then a mesh of default merit functions was chosen to optimize the illumination distribution through adjusting the normalized illumination of every mesh in the target plane. Since the variables in each zone were categorized into two parts, curvature and radius, we optimized the variables of one part each time. After completing the variables in both parts, we continued to optimize the variables in two zones. In a similar way, the variables in three zones were optimized, after which the variables in all zones were optimized altogether in order to obtain the final outcomes.

After optimization, the curvature of the sink in the middle was 0.6 mm, the curvature of the second zone was −0.05 mm, and the number of lenses was ten. The third zone was 1/4 cylinder and 1/8 sphere with a radius of 0.59 mm. The diameters of the center concave microlens and outer convex lens are 0.5 and 0.2 mm, respectively. The length and width of the bottom of the microlens array were both 2.18 mm, and the height from the origin to the center of the microlens array was kept at 1 mm. The lenses constructed of microlenses with different curvatures in 3-D space are shown in Fig. 6. Since the microlens array consists of both concave and convex shapes, we also refer to the array as heterogeneous microlenses.

C. Light Distribution After Heterogeneous Microlenses

We examined how an extra lens affected the illumination distribution of a single LED. Owing to the effect of the heterogeneous microlenses, the uniformity was much better than that of the bare LED. Fig. 7 shows the illumination distributions on a target plane of $3\,\mathrm{mm} \times 3\,\mathrm{mm}$ for the bare LED, LED with freeform lens, and LED with microlenses. The target plane was located in front of the light source of the LED at a distance of 2 mm. The normalized peak intensities were 0.08 and 0.04 for a bare LED chip and microlenses, respectively. It shows clearly that the microlenses re-distributed the center energy to the edges. The uniformity of a single LED was lower than 30%. With the use of microlenses and the freeform lens, the uniformity was improved to 92.01% and 72.59%, respectively. It was also found that the freeform lens demonstrated better performance than the

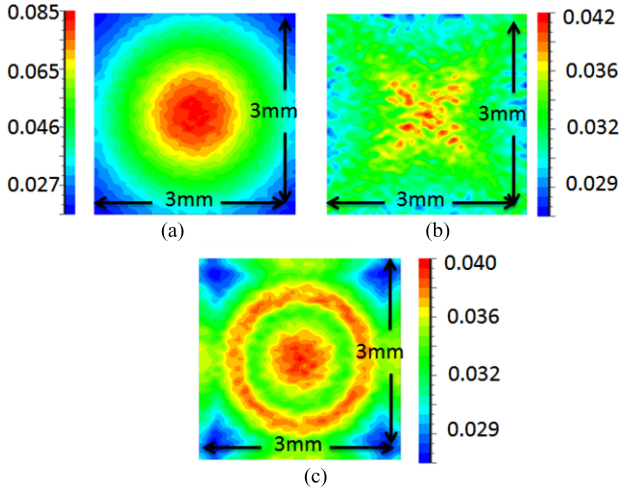

Fig. 7. Illuminance distribution for (a) bare LED (b) LED with freeform lens, and (c) LED with microlens array.

TABLE I
SIMULATED UNIFORMITY AND EFFICIENCY ON A 3 mm × 3 mm TARGET PLANE FOR ONE BARE LED, ONE LED WITH FREEFORM LENS, AND ONE LED WITH MICROLENSES

3 mm × 3 mm	Uniformity	Efficiency
Bare LED	39.40%	74.45%
Freeform lens	92.01%	73.43%
Microlenses	72.59%	67.60%

microlenses, as expected. As shown in Fig. 7(a), the uniformity and efficiency of the bare LED were 39.40% and 74.45%. The efficiency of the bare LED chip was not 100% because not all light fell onto the target plane. After the heterogeneous microlenses were placed on top of a bare LED chip, the uniformity was improved to 72.59%, at the cost of a lower efficiency of 67.60%. We can see that microlenses can improve uniformity to almost twice that of a bare LED, while the efficiency drops by only 7%. The simulated uniformity and efficiency on a 3 mm × 3 mm target plane for one bared LED, one LED with freeform lens, and one LED with microlenses are summarized in Table I.

In the optimized design, the curvature of the sink in the middle was 0.6 mm, making it a concave lens. The curvature of the second zone was −0.05 mm, making it a convex lens. The number of surrounding convex lenses was ten, as shown in Fig. 6 above. We performed tolerance analysis to study the effect of fabrication errors on microlens performance. For the center concave lens, the radius of the curvature can degrade the uniformity from 72% to 66%, as shown in Fig. 8(a). This is also true for the surrounding convex lenses; errors in the radius of the curvature of a lens can lower uniformity to about 65%, as shown in Fig. 8(b). We chose to use ten convex lenses because that number produced the best uniformity performance, as illustrated in Fig. 8(c). It is noted that within the fabrication tolerance, the uniformity should be 60% or higher; this point is discussed in the later experimental section.

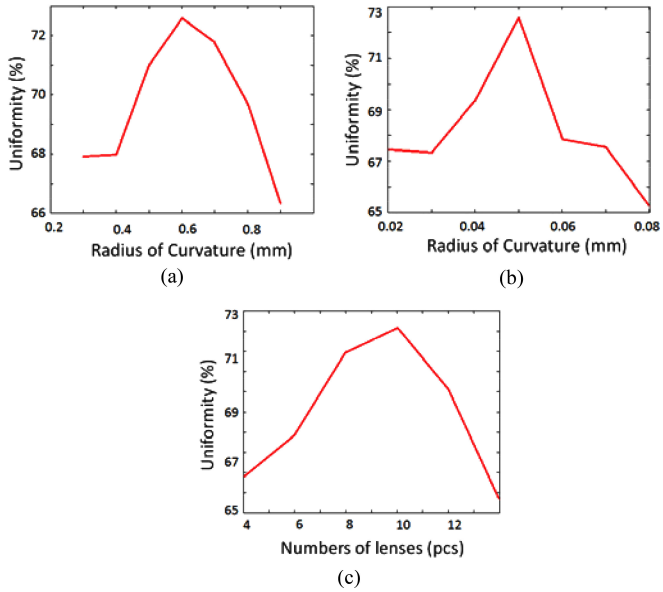

Fig. 8. Uniformity variation for (a) center concave lens (b) surrounding convex lenses, and (c) different numbers of lenses.

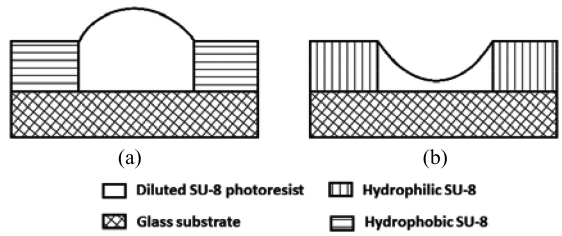

Fig. 9. Heterogeneous microlenses: (a) convex microlens with hydrophobic sidewall and (b) concave microlens with hydrophilic side wall.

III. FABRICATION OF HETEROGENEOUS MICROLENSES

In the first step of the fabrication process, we used SU-8 photoresist to build a substrate of a hollow cylinder array [15], [16]. We then used an inkjet printer and the hydrophobicity of SU-8 photoresist to fabricate a convex microlens [17], [18]. Second, we submitted the entire sample to UV/ozone treatment in order to make the SU-8 photoresist hydrophilic, including the inside of the hollow cylinder. Afterward, we returned to the process of inkjet printing. Because of the hydrophilic confinement effect, the inkjet-printed SU-8 photoresist automatically became a concave microlens, as illustrated in Fig. 9. All the processes above allowed us to fabricate a substrate with heterogeneous microlenses. The next stage was the replication process, wherein we utilized a 3-D printer to make a mold for replicating the 3-D microlenses. After assembling the substrate and the mold made with a 3-D printer, we filled the mold with polydimethylsiloxane (PDMS). Finally, we stamped the microlens arrays, as we simulated in the previous section. The details of each step in the fabrication process are described below.

In order to fabricate a microlens with a precise curvature, we need to know the relation between the volume we drop (drop

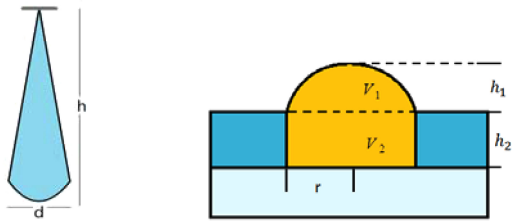

Fig. 10. Schematic drawings of droplets and microlens formation.

number) and the curvature. The first thing is to find the volume of each drop. We use d and h to describe a droplet from an inkjet printer. We also need to calculate the V_1 and V_2, or the volumes inside and outside a cavity, respectively. The curvature of a microlens is denoted as R. Formulae (7) illustrate how we calculate the volume of the microlens and the number of drops needed. Schematic drawings of a droplet and a microlens profile are provided in Fig. 10.

$$\begin{aligned} V_{\text{drop}} &= {\pi d^3}/{12} + {\pi d^2 h}/{12} \\ h_1 &= R - \sqrt{R^2 - r^2} \\ V_1 &= \pi\left(R \times h_1^2 - \frac{h_1^3}{3}\right) \\ V_2 &= \pi r^2 h_2 \\ N &= \frac{V_1 + V_2}{V_{\text{drop}}} \quad \text{(drops needed).} \end{aligned} \tag{7}$$

A. Heterogeneous Microlens Substrate

To make the substrate, a glass substrate (a cover glass) was cleaned with acetone (ACE), methanol, and isopropanol (IPA), in that order. ACE was used to clean up the organic matter, but some remained on the substrate. Methanol was used to dissolve the residual ACE. IPA, which is viscous and has a fine cleaning ability, was used to transport the organic solvents off the substrate; transportation was effected by blowing the IPA off the substrate surface with a nitrogen gun.

According to the simulation results, the substrate would have heterogeneous microlenses on its surface. In order to achieve the simulation result, it was necessary to create an array constructed of hollow cylinders of different radii. These hollow cylinders of different radii allowed us to fabricate the heterogeneous microlenses with a micro inkjet printer. Taking advantage of the high viscosity of SU-8 3035 photoresist, we spin-coated a thicker base layer on a glass substrate with SU-8 photoresist. The spin rate was 1000 r/min for 10 s and 2000 r/min for 15 s. The sample was soft baked at 95 °C for 5 min, followed by UV exposure for 26 s with an intensity of 10 mW/cm^2 before hard baking at 95 °C for 1 min. No post-exposure bake was necessary because no lithography was needed. An SU-8 photoresist base layer of about 80 μm thickness was thus formed, as shown in Fig. 11(b). After the SU-8 photoresist substrate was fabricated, we started the inkjet printing process. On account of the simulation result, we needed a convex lens in the middle of the

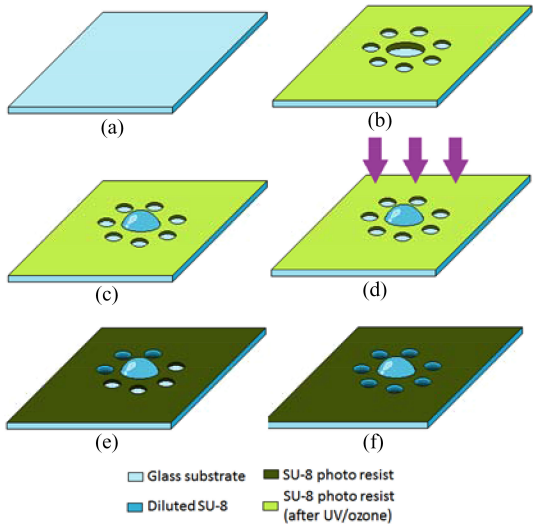

Fig. 11. Fabrication process flow of heterogeneous microlens substrate (a) glass substrate cleaned by ACE and methanol (b) spin coating a SU-8 photoresist base layer and photolithography treatment (c) inkjet printing of convex microlens (d) UV/ozone treatment (e) inkjet printing of concave microlens (f) hardening the whole sample.

microlens array on the substrate. The inkjet printer was used to form the convex microlens in the step shown in Fig. 11(c). In our case, we needed 380 drops in this step.

After the base layer and the convex microlens on the substrate were made, we put the whole sample into a UV/ozone cleaner (model UV-1, Samco) to modify the surface. The UV power was 110 W at wavelengths between 182 and 254 nm. The oxygen flow was 0.5 L/min. The processing time was fixed at 10 min, which is long enough for the SU-8 photoresist surface to reach high hydrophilicity, according to a previous report that contact angles of SU-8 photoresist on SU-8 base layer saturate at 15° after 3 min of UV/ozone treatment [19]. The hydrophilic SU-8 photoresist, including the inner wall of the cylinder, was thus formed [16]. In the next step, inkjet printing was used to fabricate the concave microlens with 10 drops, as shown in Fig. 11(e). The final step was to harden the SU-8 photoresist MLAs fabricated by inkjet printing. Since SU-8 photoresist is a negative photoresist, the heterogeneous microlenses could be hardened by UV exposure. The UV intensity for this step was 10 mW/cm^2, and the exposure time depended on the lens size. For example, the time for a center microlens with a diameter 500 μm was 5 min to ensure it was totally hardened. The hard bake step was skipped to avoid changing the lens shape.

B. Replication Process

After the heterogeneous substrate was completed, the next step was the replication process. A 3-D printed mold was designed by AutoCAD, graphics software which can be used to design 3-D graphs for a 3-D printer. The material used in the 3-D printer was plastic (ABS). The operation principle of a 3-D printer is that heat is used to melt plastic, which is then ejected onto a plate layer by layer. The advantages of a 3-D printer

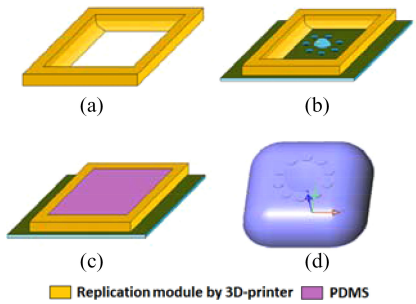

Fig. 12. Replication process (a) a replication mold made by 3-D printer (b) assembling the heterogeneous microlens substrate and the mold (c) filling the mold with PDMS (d) de-molding to remove the heterogeneous microlenses.

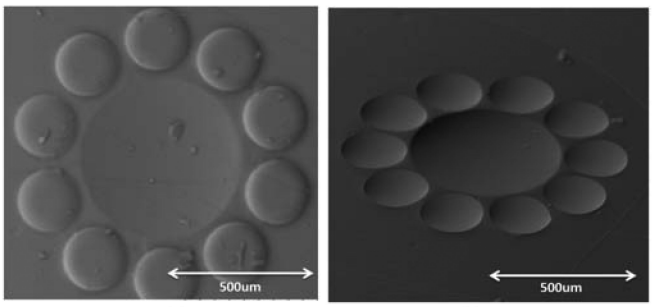

Fig. 13 (a). SEM image of top view of heterogeneous microlens (b) SEM image of high-angle view of heterogeneous microlens.

are the ease of operation, of design, and, most importantly, of production of the prototype without costly machining.

We produced a mold to develop the microlens array we simulated, one consisting of four 1/4 cylinders at the edges and four 1/8 spheres at the corners. After the mold and the substrate were combined, we filled the mold with PDMS. In the final step, hardening the PDMS, we placed the sample on a hot plate at 65 °C for an hour [20]. The schematic drawing in Fig. 12 illustrates the replication process.

IV. Experimental Results and Discussions

We successfully utilized hydrophilic and hydrophobic SU-8 photoresist and an inkjet printer to fabricate a heterogeneous microlens array. Consistent with our simulation, the inkjet printer allowed us to control the size of the lens precisely. As Fig. 13 shows, in the middle of the microlens array, we created a concave microlens with a diameter of 500 μm, which was surrounded by ten convex microlenses with diameters of 200 μm. The top view of the SEM images presents the convex and concave shapes of the microlenses.

We used a probe-type surface analyzer (Kosaka ET4000) to investigate the cross section profiles of the concave and convex lenses in Fig. 13. The measured cross section profile versus optimized design is shown in Fig. 14. Given that the printing process in Fig. 11 was performed with a home-made inkjet printer, we expected some fabrication tolerance between the fabricated and simulated heterogeneous microlenses. The measured cross

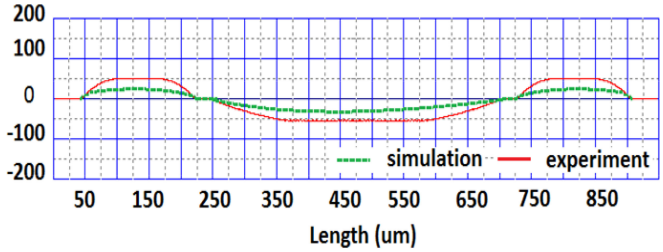

Fig. 14. The cross section profile of the fabricated microlenses (shown in solid line) versus the simulated microlenses (shown in dotted line).

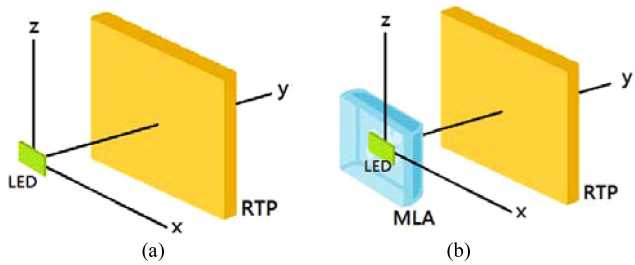

Fig. 15. The measure of light distribution and efficiency on a RTP which is 2 mm away from (a) a bare LED (b) a LED covered by microlens array.

section profile is plotted in a solid line in Fig. 14. Since we used diluted SU-8 photoresist to make the microlenses, the solvent in the photoresist evaporated during the curing process, and this may have caused some discrepancies from the predictions by equation (7). We used a printer head with only a single nozzle of diameter 30 μm. Such a small nozzle needs regular cleaning to prevent blockage. We found out that the fabricated lenses curved more than those in the original design. This can be adjusted by reducing the droplet number in the outer convex lens section. For the center convex lens area, more droplets of SU-8 photoresist were needed to make it smoother. Based on the tolerance analysis in Fig. 8, we could expect the uniformity of the LED lighting to be 60% or higher.

In non-imaging optics, there are two primary concerns in design procedures: the controlled transfer of radiation and efficiency. The main aspects of radiation transfer to solve in non-imaging optics are to maximize the transfer efficiency and create a controlled illuminance distribution [4]. Efficiency represents the proportion of the total flux emitted from the source transferred onto the target plane. It is defined as the ratio of flux on the target plane to flux emitted from the source, which is explained in a previous work [13]. The second factor is uniformity, which defines whether the illumination on the plane is uniform or non-uniform. A RTP is divided into nine areas. Uniformity is the ratio of the minimum illumination in the nine areas divided by the average of the nine areas [21].

Fig. 15(a) and (b) illustrate the measurement setups for uniformity and efficiency. As in the simulation, the target plane ($3\,\mathrm{mm} \times 3\,\mathrm{mm}$) was located in front of the light source of the LED, at a distance of 2 mm. The most crucial parameters are uniformity and efficiency. Table II compares the experimental results on uniformity and efficiency of the bare LED and the

TABLE II
EXPERIMENTAL RESULTS OF UNIFORMITY AND EFFICIENCY ON A $3\,\mathrm{mm} \times 3\,\mathrm{mm}$ TARGET PLANE FROM BARE LED AND MICROLENS-COVERED LED

$3\,\mathrm{mm} \times 3\,\mathrm{mm}$	Uniformity	Efficiency
Bare LED	17.02%	74.45%
Microlenses	63.10%	62.43%

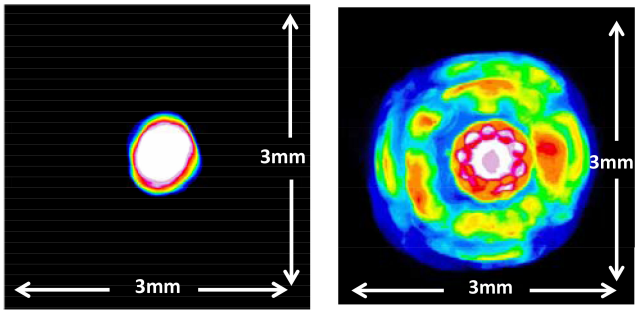

(a) (b)

Fig. 16. Light distribution on a camera of (a) bare LED and (b) LED covered with heterogeneous microlenses onto a $3\,\mathrm{mm} \times 3\,\mathrm{mm}$ target plane.

LED with a microlens array. The percentages of uniformity for the bare LED and the LED with a microlens array were 17.02% and 63.10%, respectively. This uniformity of the light distribution is close to previous predictions. Although the efficiency was reduced from 74.45% to 62.43%, a loss of about 12%, the uniformity was improved by almost a factor of 5 after microlenses were installed on top of a LED. The results on efficiency for the fabrication were also close to those of the simulation. Because the LED is embedded into the heterogeneous microlenses, there is no gap between the LED light source and the microlens array. Such a gap could cause internal reflection, which could lower efficiency. This design has a huge impact on efficiency.

The main purpose of the heterogeneous microlenses is to redistribute the light intensity from an LED. Fig. 16 shows the light distribution on a camera with a $3\,\mathrm{mm} \times 3\,\mathrm{mm}$ image plane of a bare LED and an LED covered by a microlens array. We discovered that the light distribution was much more uniform when the LED was covered by heterogeneous microlenses. Not only is the center peak lower for the LED with heterogeneous microlenses, but also the illuminated area is increased as well.

V. CONCLUSION

We have demonstrated a simple method for fabricating a PDMS microlens array to replace the freeform lens. The process is simple, low in cost, and duplicable. We use a hydrophilic confinement effect and an inkjet printer to control the dimensions of the heterogeneous microlenses. A 3-D printer is used to fabricate the mold for the replication process. In this work, we demonstrate that micro structures on top of LEDs can be made by inkjet printers, in principle. We have successfully fabricated heterogeneous microlenses to redistribute the light intensity from an LED chip. When the LED is coated with the microlens array (the area of the microlenses being $2\,\mathrm{mm} \times 2\,\mathrm{mm}$), the light distribution is more uniform than that of a bare LED. Experimental results show that uniformity is improved approximately from 17% to 63%. Moreover, the uniformity can be improved through superposition, meaning that the light distribution could be made more uniform with a larger array. This will be useful for the backlight units of LCD or any other applications needing uniform light distribution.

REFERENCE

[1] K. Wang *et al.*, "Design of compact freeform lens for application specific light-emitting diode packaging," *Opt. Exp.*, vol. 18, no. 2, pp. 413–425, 2010.
[2] Z. Feng *et al.*, "Design of LED freeform optical system for road lighting with high luminance/illuminance ratio," *Opt. Exp.*, vol. 18, no. 21, pp. 22020–22031, 2010.
[3] H. Cho *et al.*, "A local dimming algorithm for low power LCD TVs using edge-type LED backlight," *IEEE Trans. Consum. Electron.*, vol. 56, no. 4, pp. 2054–2060, Nov. 2010.
[4] G. Harbers *et al.*, "LED backlighting for LCD HDTV," *J. SID*, pp. 347–350, 2002.
[5] C. Lai *et al.*, "Structural effects on highly directional far-field emission patterns of GaN-based micro-cavity light-emitting diodes with photonic crystals," *J. Lightw. Technol.*, vol. 28, no. 19, pp. 2881–2889, Oct. 2010.
[6] D. Wu *et al.*, "Enhancement of light extraction of multi-chips light-emitting diode (LED) modules with various micro-structure arrays," in *Proc. 11th Int. Conf. Electron. Packag. Technol. High Density Packag.*, 2010, pp. 1398–1400.
[7] S.-C. Shei, "Multiple nanostructures on full surface of GZO/GaN-based LED to enhance light-extraction efficiency using a solution-based method," *IEEE J. Quantum Electron.*, vol. 50, no. 8, pp. 629–632, Aug. 2014.
[8] X.-Hao Lee *et al.*, "Highly energy-efficient agricultural lighting by B+R LEDs with beam shaping using micro-lens diffuser," *Opt. Commun.*, vol. 291, pp. 7–14, 2013.
[9] M. Tsai *et al.*, "Efficiency enhancement and beam shaping of GaN–InGaN vertical-injection light-emitting diodes via high-aspect-ratio nanorod arrays," *IEEE Photon. Technol. Lett.*, vol. 21, no. 4, pp. 257–259, Feb. 2009.
[10] D. Michael *et al.*, "Directional control of light-emitting-diode emission via a subwavelength-apertured metal surface," *IEEE Photon. Technol. Lett.*, vol. 18, no. 21, pp. 2197–2199, Nov. 2006.
[11] YI Luo *et al.*, "Design of compact and smooth free-form optical system with uniform illuminance for LED source," *Opt. Exp.*, vol. 18, no. 9, pp. 9055–9063, 2010.
[12] F. Chen *et al.*, "Free-form lenses for high illumination quality light-emitting diode MR 16 lamps," *Opt. Eng.*, vol. 48, pp. 123002–1–123002–7, 2009.
[13] B. Parkyn *et al.*, "Free-form illumination lenses designed by a pseudo-rectangular lawnmower algorithm," *Proc. SPIE*, vol. 6338, pp. 633808–1–633808–7, 2006.
[14] L. Wang *et al.*, "Discontinuous free-form lens design for prescribed irradiance," *Appl. Opt.*, vol. 46, pp. 3716–3723, 2007.
[15] C. Chang *et al.*, "Fabrication of a SU-8-based polymer-enclosed channel with a penetrating UV/ozone-modifled interior surface for electrokinetic separation of proteins," *J. Micromech. Microeng.*, vol. 20, art. no. 115031, 2010.
[16] H. Wei *et al.*, "Fabrication of transparent and self-assembled microlens array using hydrophilic effect and electric fielding pulling," *J. Micromech. Microeng.*, vol. 22, art. no. 025007, 2012.
[17] R. Förch *et al.*, *Surface Design: Applications in Bioscience and Nanotechnology*. New York, NY, USA: Wiley, 2009.
[18] E. Park *et al.*, "New fabrication technology of convex and concave microlens using UV curing method," in *Proc. IEEE Annu. Meet. Lasers Electro-Opt. Soc.*, 1999, vol. 2, pp. 639–640.
[19] H. Wei *et al.*, "Using hydrophilic effect to fabricate self-assembled microlens array by UV/ozone modification," *IEEE Photon. Technol. Lett.*, vol. 24, no. 4, pp. 300–302, Feb. 2012
[20] P. Qu *et al.*, "A simple route to fabricate artificial compound eye structures," *Opt. Exp.*, vol. 20, no. 5, pp. 5775–578, 2012.
[21] R. Chang *et al.*, "LED backlight module by lightguide-diffusive component," *J. Disp. Technol.*, vol. 8, no. 2, pp. 79–86, 2012.

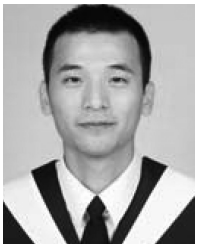

Cheng-Han Chiang was born in Hsinchu, Taiwan, in 1988. He received the B.S. degree from Yuan Ze University, Taoyuan, Taiwan, in 2012. He is currently working toward the M.S. degree at the Graduate Institute of Photonics and Optoelectronics, National Taiwan University, Taipei, Taiwan. His research interests include optical MEMS elements designs and fabrications.

Guo-Dung John Su received the B.S. degree from the National Taiwan University, Taipei, Taiwan, in 1994, and the M.S. and Ph.D. degrees in electrical engineering from the University of California at Los Angeles, Los Angeles, CA, USA, in 1998 and 2001, respectively. His Ph.D. research interests include MEMS scanners with flat mirror surface for active optical alignment and micromirror arrays for adaptive optics applications. Since 2004, he has been an Assistant Professor at the Department of Electrical Engineering, Graduate Institute of Photonics and Optoelectronics, National Taiwan University. His current research interests include MEMS devices for optical communications, compact optical imaging systems, and surface plasmon phenomenon on nanoparticles.